AGU PUBLICATIONS

JGR

Journal of Geophysical Research: Atmospheres

RESEARCH ARTICLE
10.1002/2017JD027845

Quantifying Water and Energy Fluxes Over Different Urban Land Covers in Phoenix, Arizona

Nicole P. Templeton[1], Enrique R. Vivoni[1,2], Zhi-Hua Wang[1], and Adam P. Schreiner-McGraw[2]

[1]School of Sustainable Engineering and the Built Environment, Arizona State University, Tempe, AZ, USA, [2]School of Earth and Space Exploration, Arizona State University, Tempe, AZ, USA

Key Points:
- Urban measurements indicate that differences in net radiation are attributed due to land cover variations in albedo and shallow soil temperature
- Partitioning of available energy between sensible and latent heat fluxes was modulated strongly by the presence of outdoor water use
- Decoupling between energy partitioning and precipitation indicates urban irrigation removes water limitations on the energy balance

Correspondence to:
E. R. Vivoni,
vivoni@asu.edu

Citation:
Templeton, N. P., Vivoni, E. R., Wang, Z.-H., & Schreiner-McGraw, A. P. (2018). Quantifying water and energy fluxes over different urban land covers in Phoenix, Arizona. *Journal of Geophysical Research: Atmospheres*, *123*, 2111–2128. https://doi.org/10.1002/2017JD027845

Received 4 OCT 2017
Accepted 6 FEB 2018
Accepted article online 13 FEB 2018
Published online 23 FEB 2018

Abstract The impact of urbanization on water and energy fluxes varies according to the characteristics of the urban patch type. Nevertheless, urban flux observations are limited, particularly in arid climates, given the wide variety of land cover present in cities. To help address this need, a mobile eddy covariance tower was deployed at three locations in Phoenix, Arizona, to sample the surface energy balance at a parking lot, a xeric landscaping (irrigated trees with gravel) and a mesic landscaping (irrigated turf grass). These deployments were compared to a stationary eddy covariance tower in a suburban neighborhood. A comparison of the observations revealed key differences between the mobile and reference sites tied to the urban land cover within the measurement footprints. For instance, the net radiation varied substantially among the sites in manners consistent with albedo and shallow soil temperature differences. The partitioning of available energy between sensible and latent heat fluxes was modulated strongly by the presence of outdoor water use, with the irrigated turf grass exhibiting the highest evaporative fraction. At this site, we identified a lack of sensitivity of turbulent flux partitioning to precipitation events, which suggests that frequent outdoor water use removes water limitations in an arid climate, thus leading to mesic conditions. Other urban land covers with less irrigation, however, exhibited sensitivity to the occurrence of precipitation, as expected for an arid climate. As a result, quantifying the frequency and magnitude of outdoor water use is critical for understanding evapotranspiration losses in arid urban areas.

1. Introduction

As cities continue to grow worldwide, the transformation of natural environments into urban land covers will accelerate (United Nations, 2015). Urban land use typically exemplifies a shift to impervious land cover, including concrete, asphalt, gravel cover, and buildings, and landscaping that involves native and nonnative plants (e.g., Cook et al., 2012; Grimm et al., 2008; Wu et al., 2011). The outdoor water supporting urban vegetation in arid regions where precipitation is infrequent, for instance, promotes a higher degree of plant biodiversity (Buyantuyev & Wu, 2012; Hope et al., 2003), improves the local thermal comfort (Gober et al., 2010; Song & Wang, 2015), affects the soil water balance (Volo et al., 2014, 2015), and induces higher evaporative losses (Liang et al., 2017; Litvak et al., 2017). Modeling studies have also shown that the material, thermal, and hydrologic properties of urban surfaces, such as roofs, green spaces, and buildings, impact energy and water exchanges with the atmosphere (e.g., Arnfield, 2003; Benson-Lira et al., 2016; Georgescu et al., 2009; Grimmond & Oke, 2002; Grimmond et al., 2010; Lee et al., 2012; Shaffer et al., 2015; Yang et al., 2016). Intraurban studies have been conducted in European cities (Christen & Voogt, 2004; Offerle et al., 2006) to explore energy partitioning and the surface energy balance (SEB), with an emphasis on comparing across different urban land covers and to nearby rural areas. Nevertheless, few studies have observed the effects of different types of urban land covers on the SEB in arid and semiarid environments and the partitioning of turbulent fluxes in a comparative manner such that the effects of precipitation and outdoor water use can be discerned (e.g., Best & Grimmond, 2016; Coutts et al., 2007; Liang et al., 2017).

Understanding the links between urban land cover and the SEB processes that influence microclimatic conditions is critical for planning and design purposes (Georgescu et al., 2015; Middel et al., 2012; Mitchell et al., 2008; Wang et al., 2016), in particular, for cities facing an urban heat island. In the Phoenix, Arizona, metropolitan area, rapid urbanization during the second half of the twentieth century led to the conversion of agriculture and desert lands into urban and suburban developments (e.g., Hirt et al., 2008; Jenerette et al., 2011). Due to low annual precipitation amounts, urbanization was accompanied by outdoor water use in residential, commercial, and recreational areas based upon different strategies, including mesic (sprinkler irrigated turf

grass) and xeric (drip irrigated trees with gravel cover) landscaping (e.g., Song & Wang, 2015; Volo et al., 2014; Yang & Wang, 2015). The use of outdoor water for vegetated landscaping also ameliorates, to some extent, the urban heat island effect (Buyantuyev & Wu, 2010; Gober et al., 2010; Norton et al., 2015). While the cooling properties of urban green spaces are recognized, quantitative studies on the effect of residential landscaping on surface energy fluxes, including evapotranspiration, are relatively rare (cf. Coutts et al., 2007; Goldbach & Kuttler, 2013; Litvak & Pataki, 2016) with most prior work relying on quantitative relations between urban temperature and measures of the cooling potential of different land covers (see Jenerette et al., 2011; Middel et al., 2015).

Meteorological flux measurements using the eddy covariance (EC) technique provide a detailed quantification of SEB processes and their interactions with atmospheric and land surface conditions (e.g., Anderson & Vivoni, 2016; Baldocchi et al., 1988; Wilson et al., 2002). Urban flux measurements, however, are challenging due to deployment logistics, security concerns, and the ability to take measurements without disrupting typical activity (Grimmond, 2006; Kotthaus & Grimmond, 2012). Nevertheless, there is a need for urban flux observations in arid and semiarid climates (Grimmond & Christen, 2012), in particular, for different types of urban land cover patches captured in the footprint of EC measurements (Grimmond et al., 2010; Loridan & Grimmond, 2012). The EC footprint, or source area, is a time-variable land surface area that directly contributes to the flux measurements and is a function of atmospheric conditions, the measurement height, and urban roughness properties (Grimmond, 2006; Schmid, 1994). Recent studies using EC footprint measurements in different urban areas, for example, have identified the role of irrigated vegetation on evapotranspiration (Chow, Volo, et al., 2014), the effect of urban density on heat storage (Christen & Voogt, 2004; Coutts et al., 2007; Offerle et al., 2006), and the increase in anthropogenic heat emissions after urbanization (Hong & Hong, 2016).

In this study, we use a trailer-mounted (mobile) EC tower to measure meteorological fluxes and the SEB in three urban settings within Arizona State University (ASU) in the Phoenix metropolitan area. These short-term deployments (average duration of 57 days each) in the winter, early summer, and North American monsoon (NAM, July–September) seasons are compared to a stationary (reference or REF) EC tower located in a suburban neighborhood and spanning the entire sampling period of 273 days (1 January to 30 September 2015). The three mobile sites represent different urban land cover types or patches (i.e., xeric landscaping (XL), parking lot (PL), and mesic landscaping (ML)) that are expected to vary in terms of the SEB and the partitioning of turbulent fluxes due to variations in urban materials, outdoor water use, and the morphology of the built environment. In all deployments, the EC measurements were designed to capture turbulent fluxes for the characteristic urban patch inside the EC footprint without extending to the neighborhood scale, which consists of a heterogeneous mosaic of different types of urban land cover. Thus, the objectives of this effort are to (1) quantify and compare the SEB processes over different urban land cover types in relation to a reference location in an arid environment and (2) relate the differences in the observed SEB metrics to the land cover characteristics in the flux measurement source area. A focus is placed on the role of precipitation events and outdoor water use on modifying the partitioning of the turbulent fluxes to capture how the linkage of the energy and water balances varies across the sites.

2. Methods

2.1. Study Sites and Their Characteristics

The study sites are in the Phoenix metropolitan area, which has a population of approximately 4.1 million as of 2010 (U.S. Census Bureau, 2010). Due to its location in the Sonoran Desert, Phoenix, has a hot, arid climate (Koppen classification BWh) that has been underrepresented with respect to urban flux measurements (Chow, Volo, et al., 2014). Average annual temperature is 24°C at the Phoenix Sky Harbor International Airport (PHX), with seasonal average temperatures of 14.1, 22.9, 33.9, and 24.8°C, for winter, spring, summer, and fall. The precipitation regime is bimodal with winter frontal storms and summer thunderstorms during the NAM (Adams & Comrie, 1997; Vivoni et al., 2008). Mean annual precipitation is 204 mm/yr based on observations from 1981 to 2010 at PHX, with winter (December–February) and summer (July–September) amounts of 68.3 mm and 67.8 mm, respectively. Spring and early summer (March–June) are typically dry accounting for only 17% of the mean annual precipitation.

Each deployment site represents a common type of urban land cover in Phoenix. Table 1 summarizes site characteristics, including the Local Climate Zone (LCZ) classification of Stewart and Oke (2012), while

Table 1
General Characteristics for the Four Study Sites

Site	Land cover	LCZ	UTM easting (m)	UTM northing (m)	Latitude	Longitude	Elevation (m)
XL	Xeric landscaping	LCZ 5	413,797	3,698,213	33.4198°	−111.9272°	354
PL	Pavement	LCZ 8	412,725	3,698,373	33.4212°	−111.9387°	356
ML	Mesic landscaping	LCZ 9	436,646	3,686,041	33.3116°	−111.6806°	411
REF	Residential	LCZ 6	393,794	3,705,539	33.4838°	−112.1426°	337

Note. XL = xeric landscaping; PL = parking lot; ML = mesic landscaping; REF = suburban residential; LCZ = Local Climate Zone; UTM = Universal Transverse Mercator.

Figure 1 indicates their location and provides a photograph of each EC tower. The XL site, placed during the winter months on the ASU Tempe campus (Figure 1d), was composed of palo verde (*Parkinsonia florida*) trees with gravel and bare soil cover (undeveloped). Trees were irrigated using a drip system and ranged in height from 3 to 4 m, located within setting that included a midrise (three-story) building and a paved road (LCZ 5). In contrast, the PL site on the ASU Tempe campus was a large pavement area with a small proportion of gravel cover (undeveloped) and minimal trees (Figure 1c), deployed during the early summer. The PL is near an intersection with high traffic and frequently contained vehicles, with a low number of 6 m palm trees and large low-rise (one- to three-story) buildings surrounded by impervious cover nearby (LCZ 8). The ML site was installed at the ASU Polytechnic campus (Figure 1e) during the summer and consisted of a regularly irrigated turf grass area using a sprinkler system (approximately 2–3 days per week, 3 times per day, for 20 to 30 min each time), with sparse, undeveloped land cover nearby. The large grassy area is located among a series of low-rise (one-story), single-family homes with undeveloped and pervious landscaping, including sparse 6 m trees (LCZ 9), previously used to investigate microclimatic and soil moisture conditions in residential yards (Martin et al., 2007; Volo et al., 2014). All of the deployment sites are in the built environment such that bare soil conditions are disturbed, generally consist of light-colored, coarse-grained (sandy to sandy loam) textures and have partial gravel cover from landscaping activities. The REF site represents a suburban residential area in Phoenix consisting of single-family homes, streets, open spaces, and other buildings (Figure 1b, LCZ 8). The EC deployment at the REF site is described by Chow, Volo, et al. (2014). In this study, the REF site is a reference location that encompasses the entire period and allows comparisons to the shorter deployments at each mobile EC site, as described next.

2.2. Eddy Covariance Measurements and Data Processing

The mobile EC platform consists of a telescoping tower that extends to a maximum height of 15 m. In this study, EC measurements were carried out at a height of 7.0 (XL), 9.0 (PL), and 8.0 m (ML) to ensure that fluxes were observed within the surface layer and above the zero plane displacement heights. High-frequency turbulent fluxes were measured using an open-path infrared gas analyzer and a three-dimensional sonic anemometer (Table 2) and aligned to the dominant wind direction for each deployment. Dominant wind directions were determined from wind rose diagrams from meteorological stations on the ASU Tempe campus for the XL and PL sites and from a nearby airport (~1 km) for the ML site. Site conditions were inspected to select the measurement height for each case to obtain sensible and latent heat fluxes above the average height of the urban land cover of interest while maintaining a relatively small EC footprint. The REF site, however, had a taller height of 22.1 m intended to sample fluxes from a broader area (Chow, Volo, et al., 2014). Measurements were sampled at frequencies of 10 or 20 Hz (Table 3), recorded with a data logger (CR5000, Campbell Scientific) and processed at 30 min intervals using the EdiRE software program (Clement, 1999). EC processing was performed consistently for all sites and included correcting for fluctuations in stability (Foken, 2006) and density (Webb et al., 1980), using the sonic temperature to calculate sensible heat flux (Paw U et al., 2000), rotating the coordinate frame to set the mean vertical wind speed to zero during each 30 min interval (Wilczak et al., 2001) and removing signal lags in the gas concentrations (Massman, 2001). Flux data were also filtered to exclude periods with precipitation ($>$0.2 mm/30 min), when the wind direction was 180° ± 10° from the direction at which instruments were mounted and for outliers greater than 3 standard deviations. Additional sensors recorded radiation, meteorological, and soil conditions as 30 min averages (Table 2). For all mobile deployments, a four-component net radiometer was installed at the same 5 m height to measure incoming and outgoing shortwave and longwave radiation. Precipitation at the mobile sites was measured at 1 m height above the soil surface using a tipping bucket rain gauge. Soil

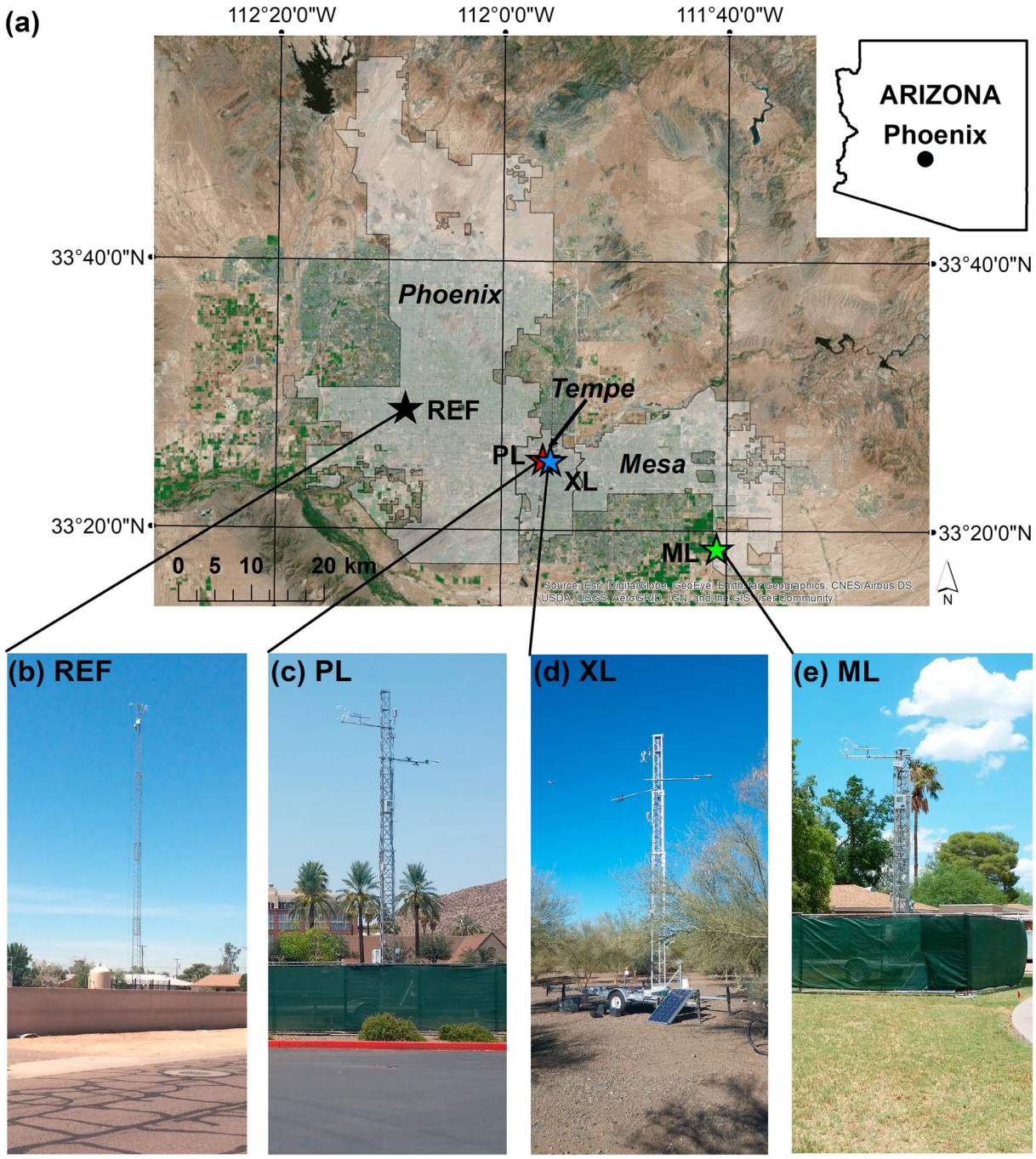

Figure 1. Four study sites located in Phoenix (a) including photographs of the EC deployments at (b) suburban (REF) site in low-rise, single-family residential area in Phoenix (c) parking lot (PL) site at ASU Tempe campus on an impervious surface near a high traffic intersection, (d) xeric landscaping (XL) site at ASU Tempe campus in a landscaping consisting of drip irrigated trees with gravel surface, and (e) mesic landscaping (ML) site near residential housing at ASU Polytechnic campus in Mesa in a landscape consisting of regularly irrigated turf grass.

moisture was measured at 5 and 50 cm depths at XL and 5, 15, and 50 cm depths at ML to quantify soil responses to precipitation and urban irrigation. Ground heat flux was measured using a heat flux plate at 5 cm depth and two thermocouples at 2 and 4 cm depths at all sites except the pavement surface at PL. Due to limitations in available equipment or access to soil for measuring ground heat flux at many sites, we only installed one sensor per deployment, except at PL where it was not possible to install a ground heat flux plate or soil temperature sensors. Average soil temperature (T_{soil}) for the 0 to 5 cm depth was

Table 2
Instrumentation at Mobile EC Tower, Including Number of Sensors in Parentheses

Instrument/model	Manufacturer	Variable measured
	Tower	
3-D sonic anemometer/CSAT3 (1)	Campbell Scientific	Three-dimensional wind velocities, virtual sonic temperature
Infrared gas analyzer/LI-7500A (1)	Li-Cor Biosciences	Water vapor and carbon dioxide concentrations
Temperature and relative humidity sensor/HMP155A (3)	Vaisala	Air temperature and relative humidity
Four-component net radiometer/CNR4 (1)	Kipp & Zonen	Incoming and outgoing shortwave and longwave radiation
Pyranometer/SP-110 (1)	Apogee Instruments	Total shortwave radiation
Barometer/CS100 (1)	Setra Systems	Barometric pressure
	Near ground level	
Rain gauge/TE525MM (1)	Texas Electronics	Precipitation
Infrared radiometer/SI-111 (1)	Apogee Instruments	Surface temperature
	Below ground level	
Soil heat flux plate/HFP01SC (1)	Hukseflux	Ground heat flux
Soil averaging thermocouple/TCAV (2)	Campbell Scientific	Soil temperature
Water content reflectometer/CS616 (3)	Campbell Scientific	Soil volumetric water content

Note. EC = eddy covariance.

determined by averaging the thermocouple measurements and the rate of change of T_{soil} was used with the soil water content to determine energy stored in the layer above the plate. Details on the setup and instruments at the REF site are found in Chow, Volo, et al. (2014).

2.3. Urban Surface Energy Balance and Meteorological Comparisons

The urban SEB is described as follows:

$$Q^* + Q_F = Q_H + Q_E + \Delta Q_S + \Delta Q_A, \tag{1}$$

where Q^* is the net radiation, Q_F is the anthropogenic heat flux, Q_H is sensible heat flux, Q_E is latent heat flux, and ΔQ_S and ΔQ_A are the net changes of heat storage and advection, all in W/m^2 (Oke, 1988). The processed turbulent fluxes and radiation, meteorological, and soil measurements were used to quantify the SEB for a simple plane facet (Arnfield, 2003) as follows:

$$Q^* - Q_G = Q_H + Q_E, \tag{2}$$

where Q_G is ground heat flux. This equation assumes that anthropogenic heat and advection are negligible and only considers the conductive heat flux from the surface (Q_G), whereas ΔQ_S represents all energy storage in the control volume. While this is not the case in urban areas (e.g., Chow, Volo, et al., 2014; Oke, 1988; Sailor, 2011), we use energy balance closure (ε) as a measure of the residual quantity ($1 - \varepsilon$) not captured by the measured fluxes:

$$\varepsilon = \frac{\Sigma(Q_H + Q_E)}{\Sigma(Q^* - Q_G)}. \tag{3}$$

Table 3
EC Deployment Specifications, Including Orientation, Height and Frequency of Turbulent Instruments and Duration of Each Deployment

Site	Orientation (deg)	Height (m)	Frequency (Hz)	Start day and time	End day and time	Total days
XL	21	7.0	20	1/20/2015 12:00	3/13/2015 8:30	53
PL	227	9.0	10	5/19/2015 15:00	6/30/2015 6:00	43
ML	230	8.0	10	7/9/2015 13:00	9/18/2015 8:30	74
REF	270	22.1	10	1/1/2015 0:00	9/30/2015 23:30	273

Note. XL = xeric landscaping; PL = parking lot; ML = mesic landscaping; EC = eddy covariance; REF = suburban residential.

Table 4
Urban Land Cover Percentages Within 80% Source Area and Radiometer Footprint

	80% source area			Radiation footprint			
Urban land cover	XL	PL	ML	XL	PL	ML	REF
Trees	38.2%	5.9%	16.2%	34.4%	2.2%	6.8%	4.6%
Grass	0.4%	0.7%	28.1%	0.0%	0.7%	43.6%	10.0%
Undeveloped	29.7%	13.9%	34.6%	65.6%	29.6%	34.5%	36.8%
Pavement	8.3%	57.4%	12.8%	0.0%	67.5%	4.1%	22.0%
Buildings or cement	23.4%	22.1%	8.3%	0.0%	0.0%	11.0%	26.4%
Percent in 500 m fetch	97.1%	94.5%	96.4%				

Note. The percentage of flux originating from a 500 m radius fetch centered at each EC site is shown. REF site information is as reported in Chow, Volo, et al. (2014). XL = xeric landscaping; PL = parking lot; ML = mesic landscaping.; REF = suburban residential.

We also compute a separate residual (RES) term to approximate an upper limit of ΔQ_S that includes Q_G (Chow, Salamanca, et al., 2014; Christen & Voogt, 2004) as follows:

$$\mathrm{RES} = Q^* - Q_H - Q_E. \tag{4}$$

For the EC systems deployed, net radiation (Q^*) is obtained from measurements of the incoming and outgoing components of shortwave ($K_\downarrow$ and $K_\uparrow$) and longwave ($L_\downarrow$ and $L_\uparrow$) radiation as follows:

$$Q^* = Q_\downarrow - Q_\uparrow = \left(K_\downarrow + L_\downarrow\right) - \left(K_\uparrow + L_\uparrow\right), \tag{5}$$

where $Q_\downarrow$ is the total incoming radiation and $Q_\uparrow$ is the total outgoing radiation. To compare observations at the sites (Loridan & Grimmond, 2012), we estimated ratios of sensible heat flux to total incoming radiation ($Q_H/Q_\downarrow$), latent heat flux to total incoming radiation ($Q_E/Q_\downarrow$) and the sum of sensible and latent heat fluxes to total incoming radiation ($(Q_H + Q_E))/Q_\downarrow$). All normalized quantities are computed after aggregation to the daily scale such that differences among sites at a higher temporal resolution are not captured. We also compared standard weather observations of air temperature (TA), precipitation (P), and vapor pressure deficit (VPD, obtained from relative humidity and air temperature) from each deployment to the REF site. Averaged diurnal cycles of Q^*, Q_G, Q_H, and Q_E were obtained over all sampled days at each site. Furthermore, we estimated the evaporative fraction (EF) at local noontime of each day and as a daily average as:

$$\mathrm{EF} = \frac{Q_E}{Q_H + Q_E}, \tag{6}$$

to provide further insight into the partitioning of turbulent fluxes in different urban land covers. Additional analyses, such as evaluating the temporal dynamics of Q^*, soil moisture, and EF, were performed for subsets of days classified as "wet" or "dry" based on the occurrence of precipitation ($P > 0.2$ mm/d) taken to be the day of and 2 days after a storm event.

2.4. Urban Land Cover Characterization and Footprint Analysis

To characterize the source areas of the flux measurements, a consistent land cover classification was performed for each mobile EC site using high-resolution (0.30 m cell size) color orthoimagery from the U.S. Geological Survey (http://lta.cr.usgs.gov/high_res_ortho). Supervised classifications were based on the red, green, and blue signatures using a maximum likelihood method in ArcGIS 10.4 (Image Classification Tool) and utilized training samples that were checked with site visits. Following prior efforts in Phoenix (e.g., Myint et al., 2011; Zhao et al., 2015), land cover was classified into five general types: (1) trees, (2) grass, (3) undeveloped (gravel or bare soil), (4) pavement, and (5) buildings or cement, which were compared against the high-resolution imagery and site visits to check for consistency. For the REF site, we employed the classification of Chow, Volo, et al. (2014) based on a 2.4 m resolution Quickbird image (Myint et al., 2011) for a circular region of 1 km^2 around the location. This analysis is well suited for the REF site where the source area is larger and more difficult to classify accurately due to the more heterogeneous distribution of urban land cover patch types. Table 4 reports on urban land cover percentages for each site, with REF indicating low-rise buildings (36.8%), undeveloped (26.4%) surface cover and a proportion of nonvegetated urban cover of 85.2%.

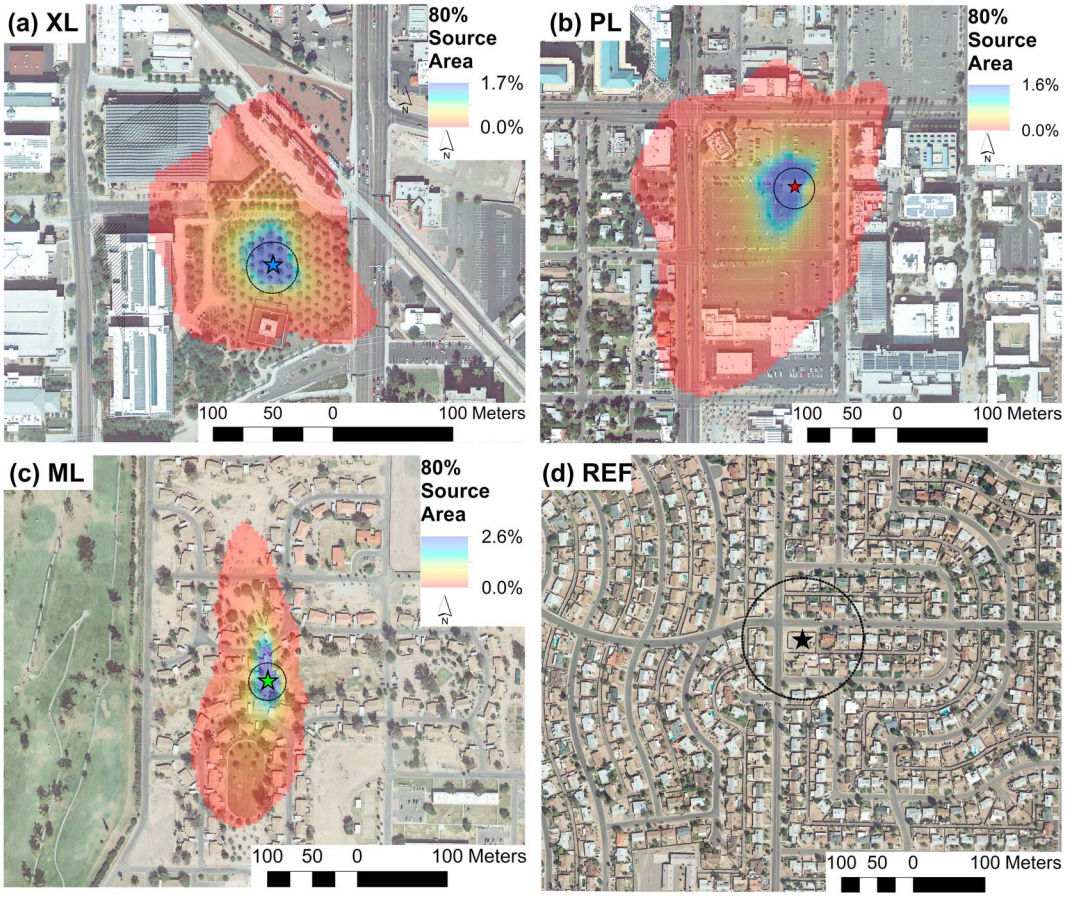

Figure 2. Study site orthoimagery with the 80% source areas (colored 5 m by 5 m pixels with percent contribution for each) and radiometer source areas (black circles) at (a) xeric landscaping (XL), (b) parking lot (PL), (c) mesic landscaping (ML), and (d) suburban residential (REF) sites.

For the mobile EC sites, we computed the percentage of each land cover class within the EC footprint and within the radiometer footprint (Table 4). The EC footprint was obtained using the analytical model of Kormann and Meixner (2001) for an area of 500 m by 500 m centered at each site and a horizontal pixel resolution of 5 m selected to be less than the measurement height (Van de Boer et al., 2013). The model is applied in the surface layer at the EC measurement height for each deployment, which is above the average tree and building heights. The surface layer consists of roughly the bottom 10% of the boundary layer, which represents a physical layer with "constant flux" arising from the land surface and can be mathematically formulated using the Monin-Obukhov Similarity Theory adopted in the model (Stull, 1988). For its operation, the model requires the measurement height, fetch radius, wind speed and direction, friction velocity, and a stability criterion. Since measurement heights were above the zero-plane displacements (2.5, 2.0, and 5.0 m at the XL, PL, and ML sites), the application of Monin-Obukhov Similarity Theory and the concept of stability are valid (Foken, 2006). Following Anderson and Vivoni (2016), the EC footprint was calculated for each 30 min interval of turbulent daytime conditions, averaged over each daytime period and aggregated to derive a unique footprint for each deployment. We selected the 80% threshold as the source area to define the EC footprint (Schmid, 1994), as shown in Figure 2 (the percent contribution of each 5 m by 5 m pixel indicated by color). While the 80% source areas appear large (red areas), most of the flux contributions are from regions near the EC towers (blue areas) and a 500 m radius contains >94% of the footprint (Table 4). In addition, we used the radiometer height to obtain an approximate circular (fixed) footprint for these measurements (Schmid et al., 1991) based on the 95% source area (or 1,492 m^2 for a 5 m height) that overlap well with the higher EC contributions. While this estimate does not account for elements of the urban environment, it is a first approximation based on flat, homogeneous terrain that is suitable for our analyses. As shown in Table 4, urban land cover distributions have similar patterns between the EC and radiometer footprints. For instance, at the XL

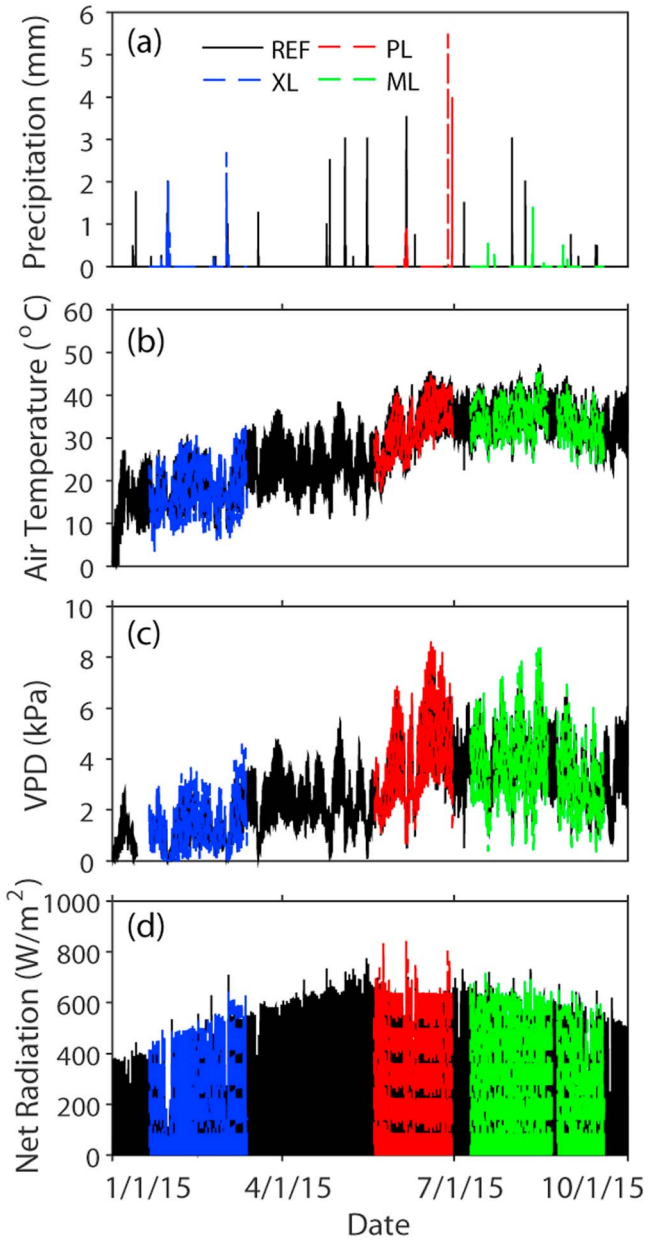

Figure 3. Comparison of meteorological measurements during entire study period (1 January to 30 September, 2015) including (a) precipitation, (b) air temperature, (c) vapor pressure deficit (VPD), and (d) net radiation, shown as 30 min averages.

site, the dominant land covers are undeveloped land in the form of gravel cover (29.7% for 80% source area and 65.6% for radiometer footprint) and trees (38.2% and 34.4%, respectively). As at other sites, this indicates that as proximity to the EC tower increases (blue areas overlapping with radiometer circle), the distribution of urban land cover types reflects the intended sampling plan and the energy balance closure of radiative and turbulent fluxes is more appropriately achieved.

3. Results and Discussion

3.1. Meteorological Conditions and Comparison to Long-Term Averages

The mobile EC deployments measured meteorological variables across a variety of urban land covers during different seasons, while the REF site spanned the entire study period. Figure 3 shows the variation of precipitation, air temperature, VPD, and net radiation. Each deployment recorded several storm events of varying intensity with observed differences in total precipitation between the mobile EC and reference sites (Table 5). For instance, the NAM season at ML exhibited a lower precipitation (5.4 mm) as compared to the REF site (13.7 mm) due to the spatial variation in timing and magnitude of individual precipitation pulses in Phoenix (Mascaro, 2016). Furthermore, the 2015 NAM season at the ML and REF sites was drier than average as compared to the long-term average at PHX (57.9 mm) with potential implications on the comparisons. In general, precipitation at all sites was lower than the long-term (1981–2010) average, except for two localized storm events on 27 and 29 June 2015 measured at the PL site (5.7 mm and 4 mm) that provided rainfall during a typically dry period of the early summer.

The temporal variations in TA, VPD, and Q^* reflect the seasonal progression from winter to summer and the effects of storm events, which tend to lower all quantities. The winter deployment at XL was characterized by low values of TA and VPD that are fairly similar to long-term averages and the REF site (Table 5). As expected, increases in TA and VPD occur in the early summer deployment at PL (red lines in Figure 3) and reach a maximum during the NAM season at ML (green lines in Figure 3). While subdaily changes in TA and VPD are consistent between each site and the reference location, small biases can be noted that are likely related to the urban land cover. For instance, the REF site is 1 to 2°C warmer than the XL and ML sites, which is consistent with the higher fraction of nonvegetated urban cover (85.2% at REF versus 61.4% and 55.7% at XL and ML, respectively). In addition, smaller differences in TA and VPD are noted between the PL (93.4% nonvegetated) and REF sites possibly due to more

Table 5
Time-Averaged Meteorological Conditions Including Measured During Each Deployment (Meas.), Conditions at REF Site (Ref.) and Long-Term Average (PHX, Observations From 1981 to 2010) for Precipitation (P), Air Temperature (TA), Vapor Pressure Deficit (VPD), and Net Radiation (Q)*

	P (mm)			TA (deg C)			VPD (kPa)			Q^* (W/m^2)		
Site	Meas.	Ref.	Long term	Meas.	Ref.	Long term	Meas.	Ref.	Long term	Meas.	Ref.	Long term
XL	38.6	27.4	43.4	16.8	18.0	15.6	1.18	1.31	0.84	68.1	61.5	—
PL	15.2	8.6	1.5	32.5	32.6	31.7	4.05	3.93	3.08	152.0	140.7	—
ML	5.4	13.7	57.9	33.6	34.5	34.0	3.46	3.73	2.82	149.2	106.8	—

Note. Long-term average Q^* is not available at PHX. XL = xeric landscaping; PL = parking lot; ML = mesic landscaping.

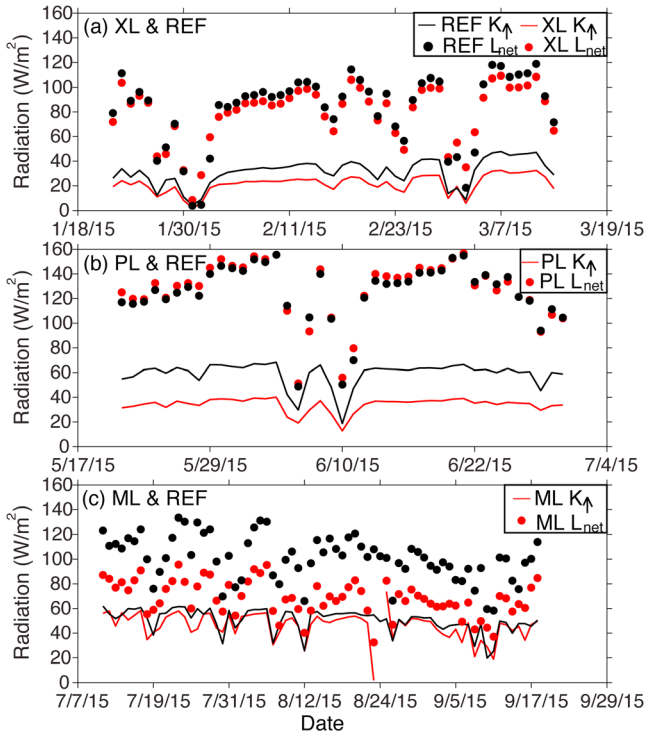

Figure 4. Comparison of daily-averaged outgoing shortwave radiation ($K_{\uparrow}$, lines) and net longwave radiation (L_{net}, dots) at (a) xeric landscaping (XL) and REF sites, (b) parking lot (PL) and REF sites, and (c) mesic landscaping (ML) and suburban residential (REF) sites. Black colors correspond to REF site, while red colors represent mobile eddy covariance sites.

similar nonvegetated urban cover fractions. Net radiation exhibits more notable differences between each site and the reference location, ranging from 7 to 43 W/m^2 lower Q^* at REF when averaged over each period (Table 5), though Pearson's correlation coefficients are high (0.97, 0.98, and 0.95 for XL, PL, and ML, respectively). Minimal differences in Q^* are observed between the XL and REF sites during the winter months when Q^* is relatively low. Larger differences among sites are observed as the year progresses in the early summer and NAM season corresponding with larger Q^* values. The lower Q^* at the REF site is linked to the urban land cover differences within the larger radiometer footprint (29,153 m^2 at REF as compared to 1,492 m^2 at mobile EC sites). Notably, the largest differences in Q^* are between the REF and ML sites where the latter is characterized by a much higher fraction of vegetation (14.6% at REF and 50.4% at ML).

3.2. Net Radiation Components and Their Link to Urban Land Cover

We inspected the outgoing shortwave ($K_{\uparrow}$) and net longwave radiation (defined as $L_{net} = L_{\uparrow} - L_{\downarrow}$ to maintain positive values) to diagnose differences in net radiation among sites. Figure 4 presents daily-averaged comparisons of $K_{\uparrow}$ (lines) and L_{net} (dots) over each deployment (winter, early summer, and NAM). $K_{\uparrow}$ is generally higher at the REF site, consistent with a lower Q^*, due to a higher albedo (a) over the urban materials in the larger radiometer footprint, as compared to the mobile EC sites. Noontime albedo measurements ($a = K_{\uparrow}/K_{\downarrow}$) averaged over each period yielded values of 0.109 (XL), 0.094 (PL), 0.167 (ML), and 0.169 (REF). Albedo computed from daily-averaged values show similar trends among the sites: 0.115 (XL), 0.100 (PL), 0.171 (ML), and 0.173 (REF), consistent with values obtained by Offerle et al. (2006) for similar land cover types. Albedo estimates also match well with the dominant urban land cover in each radiometer footprint and with values reported for the REF site by Chow, Volo, et al. (2014), where residential and more vegetated areas have higher values. While some trends are observed within each season (i.e., increasing $K_{\uparrow}$ during winter and decreasing $K_{\uparrow}$ during the NAM), the largest daily changes in $K_{\uparrow}$ correspond to the effects of storm events that moistened urban land covers and changed albedo for short periods of time (1 to 3 days). In addition, larger differences in $K_{\uparrow}$ occur between the PL (dark-colored pavement) and REF (light-colored cement and undeveloped surfaces) sites that have large albedo differences, while the most similar $K_{\uparrow}$ occurs for the ML and REF sites, which have the most similar albedo. This is consistent with urban measurements by Santillán-Soto et al. (2015) who reported much lower values of $K_{\uparrow}$ for pavement surfaces as compared to other urban land covers, including cement, grass, and clay surfaces. It also indicates that the large differences in Q^* between the ML site and the REF site during the NAM season are not due to variations of shortwave components or albedo differences.

Site comparisons of Q^* are also aided by inspecting L_{net} and its link to measured shallow soil temperature averaged from 2 and 4 cm depths (T_{soil}) at the XL, ML, and REF sites. Given similar TA for coincident deployments, differences in L_{net} can be attributed mainly to outgoing longwave radiation ($L_{\uparrow}$) and its relation to soil temperature. As with $K_{\uparrow}$, net longwave radiation exhibits trends within each season (i.e., increasing L_{net} during winter and decreasing L_{net} during the NAM) and decreases in response to storm events (Figure 4). The small offset in winter L_{net} values at the XL and REF sites (78.9 and 82.5 W/m^2, respectively) is consistent with a higher time-averaged T_{soil} at the REF site during the period (18.3 and 18.7°C, respectively). In contrast, the early summer period at PL and REF sites showed small differences in L_{net} (124.6 and 126.7 W/m^2, respectively) suggesting that the measured pavement surfaces and suburban land covers have approximately the same temperature. Thus, given the variations in albedo among the PL and REF site, the higher Q^* at the PL site is primarily due to the lower a (i.e., lower $K_{\uparrow}$), rather than a difference in L_{net}. In contrast, large variations in L_{net} during the NAM season at the ML and REF sites are due to large differences in time-averaged T_{soil} (29.7 and 41.2°C). As a result, observed differences in Q^* between the ML and REF sites are due primarily

Table 6
Energy Balance Closure Using Two Techniques: (1) Linear Fit ($Q_H + Q_E = m(Q^* - Q_G) + b$) With Slope (m), Intercept (b), and Coefficient of Determination (R^2) and (2) ε or the Ratio of the Sum of ($Q_H + Q_E$) to the Sum of ($Q^* - Q_G$)

Site	Sample size	Slope (m)	Intercept (b)	R^2	ε
XL	2,299	0.52	26.72	0.91	0.84
PL-no Q_G	1,739	0.35	50.58	0.83	0.64
PL-with Q_G	1,739	0.44	41.71	0.81	0.69
ML	2,873	0.72	33.40	0.89	0.84
REF	12,412	0.59	35.17	0.78	0.90

Note. PL site is reported with no Q_G measurement and with a surrogate Q_G from the REF site. Sample size of 30 min intervals provided for each period. XL = xeric landscaping; PL = parking lot; ML = mesic landscaping; REF = suburban residential.

to L_{net} and T_{soil} that are moderated by the urban land cover, specifically the turf grass at ML, which cools significantly under the influence of outdoor water use, in particular, near the end of summer.

3.3. Surface Energy Balance and Partitioning of Turbulent Fluxes

We inspected the energy balance closure (ε) for each site (Table 6), finding that 64–90% of the available energy ($Q^* - Q_G$) was measured as turbulent fluxes ($Q_H + Q_E$). Higher residuals ($1 - \varepsilon$) at the PL site are reduced slightly when considering Q_G from the REF site as a surrogate quantity, suggesting higher anthropogenic inputs (e.g., Salamanca et al., 2014) or other factors such as heat advection or storage (e.g., Bassett et al., 2016), as compared to the other sites. It is important to note that only one heat flux plate is installed at each site and does not represent the same spatial scale of the turbulent fluxes. Nevertheless, the estimated energy balance closure is within the range of other EC studies across different ecosystems (e.g., Wilson et al., 2002).

Figure 5 presents the averaged diurnal cycle of Q^*, Q_H, Q_E, and Q_G at 30 min intervals for each deployment, with the dashed lines representing simultaneous conditions at the REF site. Q^* follows anticipated seasonal patterns, with increasing noontime values from winter to early summer followed by a reduction during the NAM. At all mobile EC sites, the diurnal rise and peak of Q^* occurs slightly earlier due to the longitudinal

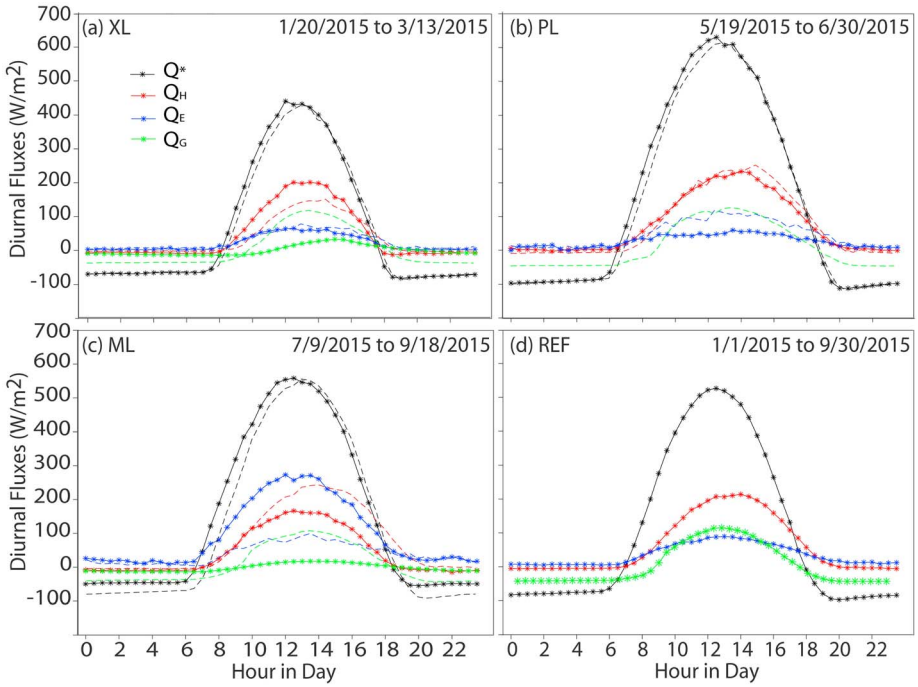

Figure 5. Averaged diurnal cycle of surface energy fluxes at 30 min intervals for the (a) xeric landscaping (XL), (b) parking lot (PL), (c) mesic landscaping (ML), and (d) suburban residential (REF) sites. For reference, dashed lines in Figures 5a–5c represent the corresponding measurements at the REF site. The PL site does not have Q_G measurements.

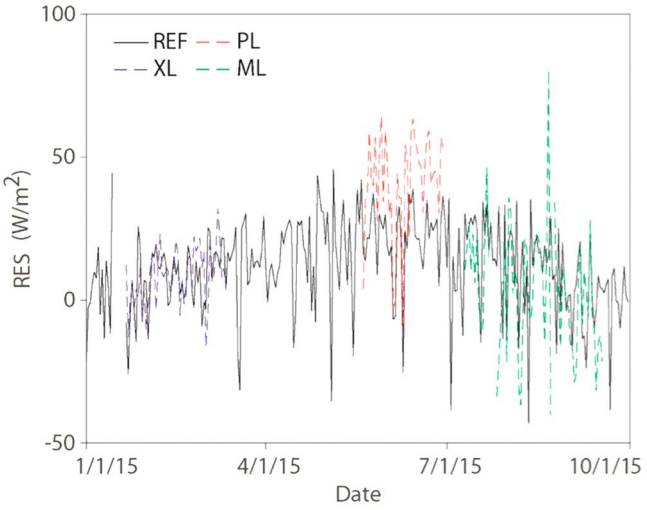

Figure 6. Daily residual (RES) computed at the xeric landscaping (XL), parking lot (PL), mesic landscaping (ML), and suburban residential (REF) sites.

distance to the reference site, located 42.8 km west of ML. The partitioning of Q^* is dominated by Q_H at all sites, except ML, with Q_H exhibiting a diurnal peak that is delayed by 1.1 h with respect to Q^* when averaged over all sites. The smaller Q_G peak exhibits a larger delay, averaging 1.7 h after Q^* over all sites, though it tends to be earlier and of greater magnitude at REF where the sensor is placed in an unshaded bare area. While the delayed Q_G peaks may be biased by the placement of the ground heat flux sensors, other studies have noted a peak in Q_G after Q^* (e.g., Ma et al., 2005; Templeton et al., 2014; Wang & Mitsuta, 1992). Interestingly, the frequent outdoor water use and mesic landscaping substantially increases Q_E relative to the REF site (i.e., by 174.2 W/m^2 for peak Q_E values in Figures 5c and 5d), leading to a substantial reduction in Q_H and Q_G during the NAM. Comparisons of Q_E at the other sites indicate that winter water input (irrigation and precipitation) has a similar impact at XL and REF. The XL site received more precipitation (11.2 mm) and was regularly irrigated, while the REF site was dependent on outdoor water use in residences and open spaces. In contrast, the early summer has a higher Q_E at the REF site as compared to the PL site, which had higher precipitation but low to negligible outdoor water use.

To further investigate the energy balance components, a daily residual (RES) term was compared across sites (Figure 6). The RES term represents an upper limit of ΔQ_S since it includes any underestimations of Q_H and Q_E

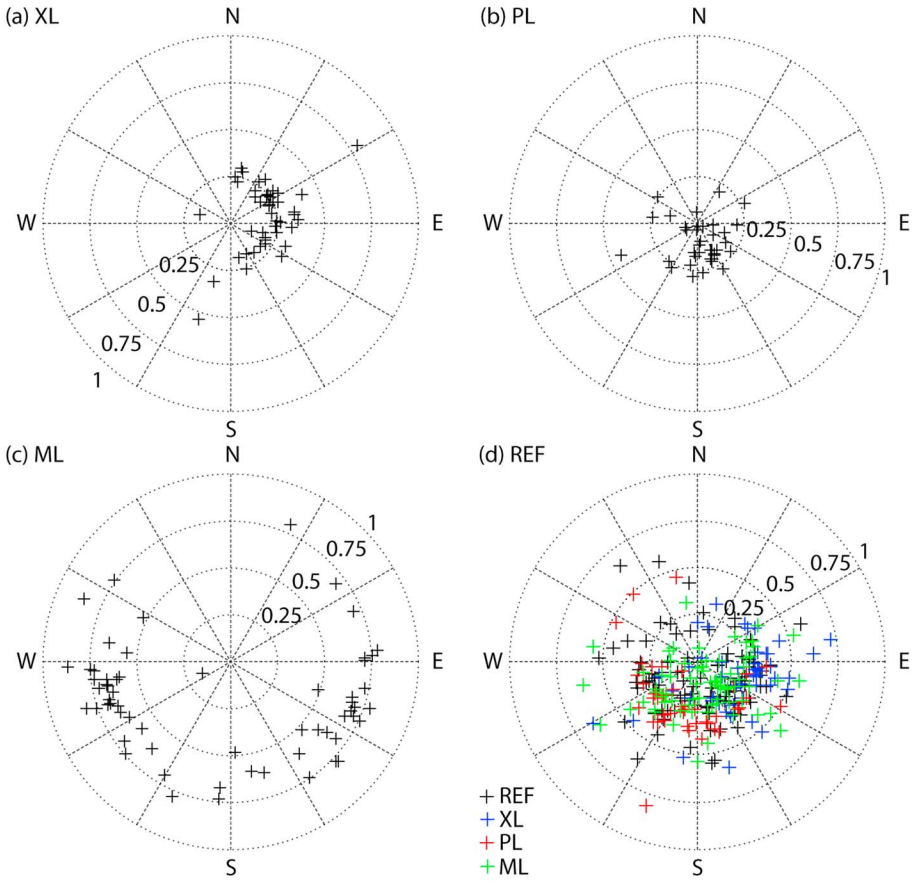

Figure 7. Radial diagrams of daily evaporative fraction (varying from zero to one) at noontime with respect to wind direction for the: (a) xeric landscaping (XL), (b) parking lot (PL), (c) mesic landscaping (ML), and (d) suburban residential (REF) sites. Color coding in Figure 7d depicts overlapping observations during deployments at the other sites or intervening periods (black, labeled REF).

Table 7
Comparison of Normalized Surface Fluxes Averaged Over Each Deployment Period, Including Evaporative Fraction Determined at Noontime (EF_{noon}) and Evaporative Fraction Averaged Over Daytime Periods (EF_{day})

Site	$Q_H/Q_\downarrow$	$Q_E/Q_\downarrow$	$(Q_H + Q_E)/Q_\downarrow$	EF_{noon}	EF_{day}
XL	0.145	0.097	0.242	0.27	0.27
PL	0.206	0.073	0.279	0.16	0.22
ML	0.132	0.302	0.434	0.61	0.64
REF	0.172	0.108	0.280	0.29	0.32

Note. XL = xeric landscaping; PL = parking lot; ML = mesic landscaping; EF = evaporative fraction; REF = suburban residential.

(i.e., the energy balance closure problem) and other terms of the urban energy balance (Q_F, Q_G, ΔQ_S, and ΔQ_A). RES increases at the REF site from the winter months into the early summer but starts to decrease during the NAM until relatively low values are obtained in September. The seasonal variation of RES is consistent with changes in ground heat flux (Q_G) included in ΔQ_S as well as heat storage in other elements of the urban environment (e.g., buildings, trees, and impervious surfaces). At the XL site, the RES term matches very well with estimates at the REF site, with similar averages of 8.4 and 7.6 W/m^2 during the deployment period, respectively, indicating a similar amount of ΔQ_S. In contrast, RES at the PL site is twice as large as compared to the REF site (average values of 41.1 and 22.2 W/m^2), suggesting that a higher ΔQ_S is likely at the PL site due to the large percentage of pavement cover. Similarly, the differences in RES between the ML and REF sites are appreciable, with a lower time-averaged RES term at ML as compared to the REF site (4.5 and 8.7 W/m^2), which is linked to the lower capacity for heat storage in frequently irrigated mesic landscaping.

As a measure of turbulent flux partitioning, the evaporative fraction (EF_{noon}) was evaluated at noontime and averaged for all days of each deployment period. Figure 7 shows the daily EF_{noon} as a function of wind direction, which can be related to the urban land cover around each site. We also computed averaged daytime (10:00 a.m. to 2:00 p.m.) EF (EF_{day}) for each site and then averaged these values over the deployment periods. Consistent with prior analyses, EF_{noon} and EF_{day} vary from low values over the pavement surface (PL) to high values in the turf grass (ML), as shown in Table 7 for averaged conditions. In addition, the EF_{noon} at each site is similar for all sampled wind directions, indicating that EF_{noon} is homogeneous with respect to the land cover in each EC footprint. Note that some wind directions were not sampled at the mobile EC sites (e.g., north at ML), but the longer period at the REF site could capture contributions from all directions. This also explains the larger variability in EF_{noon} at the REF site where the observations spanned several seasons, resulting in an average EF_{day} of 0.32, which is higher than at XL and PL (Table 7). A comparison across the sites at the daily scale also reveals that ML has a consistently higher EF_{day}, and XL and PL have a lower EF_{day}, with respect to the REF site.

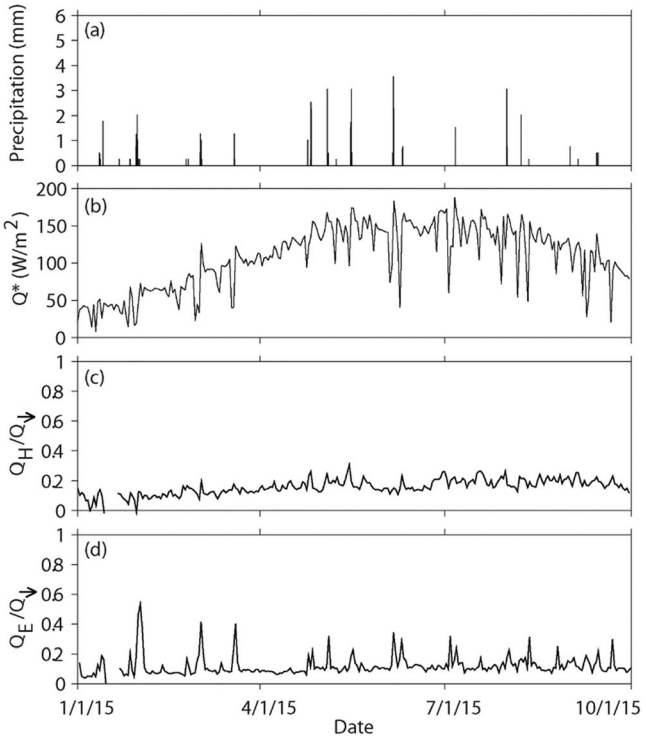

Figure 8. Meteorological variables and fluxes at the REF site: (a) precipitation and averaged daily (b) net radiation (Q^*) and turbulent heat flux ratios of (c) $Q_H/Q_\downarrow$ and (d) $Q_E/Q_\downarrow$.

Average daily turbulent heat flux ratios were evaluated for the duration of the REF period (Figure 8). Although Q^* increases substantially as the year progresses, the sensible heat ratio has a small increase, with average values of $Q_H/Q_\downarrow$ = 0.11 (winter), 0.17 (early summer) and 0.21 (NAM). There is higher variability in the latent heat flux ratio due to precipitation, but seasonal averages are nearly identical at $Q_E/Q_\downarrow$ = 0.10 (winter), 0.11 (early summer), and 0.12 (NAM). Similar seasonal values of $Q_E/Q_\downarrow$ above 0 in an arid climate are a strong indicator of the contribution of outdoor water use on turbulent heat fluxes. The response of $Q_E/Q_\downarrow$ to storm events at the REF site further shows that water limitations to evapotranspiration are still present. Table 7 complements this comparison with $Q_H/Q_\downarrow$, $Q_E/Q_\downarrow$, and $(Q_H + Q_E)/Q_\downarrow$ averaged over each deployment period. Consistent with the prior analysis, the PL site has the lowest $Q_E/Q_\downarrow$ and the highest $Q_H/Q_\downarrow$, indicating that the pavement surface primarily channels available energy into sensible heat flux (low EF). The sprinkler irrigated turf grass (ML) exhibits the opposite trends (e.g., lowest $Q_H/Q_\downarrow$ and highest $Q_E/Q_\downarrow$) with a dominance of latent heat flux (high EF). In addition, ML had the highest $(Q_H + Q_E)/Q_\downarrow$, indicating that available energy was more efficiently converted into turbulent fluxes, as opposed to Q_G, $K_\uparrow$ or $L_\uparrow$, for the ML site.

3.4. Sensitivity of Turbulent Fluxes to Precipitation and Outdoor Water Use

To evaluate the sensitivity of turbulent fluxes to wetness conditions, we classified each day as either wet or dry depending on precipitation

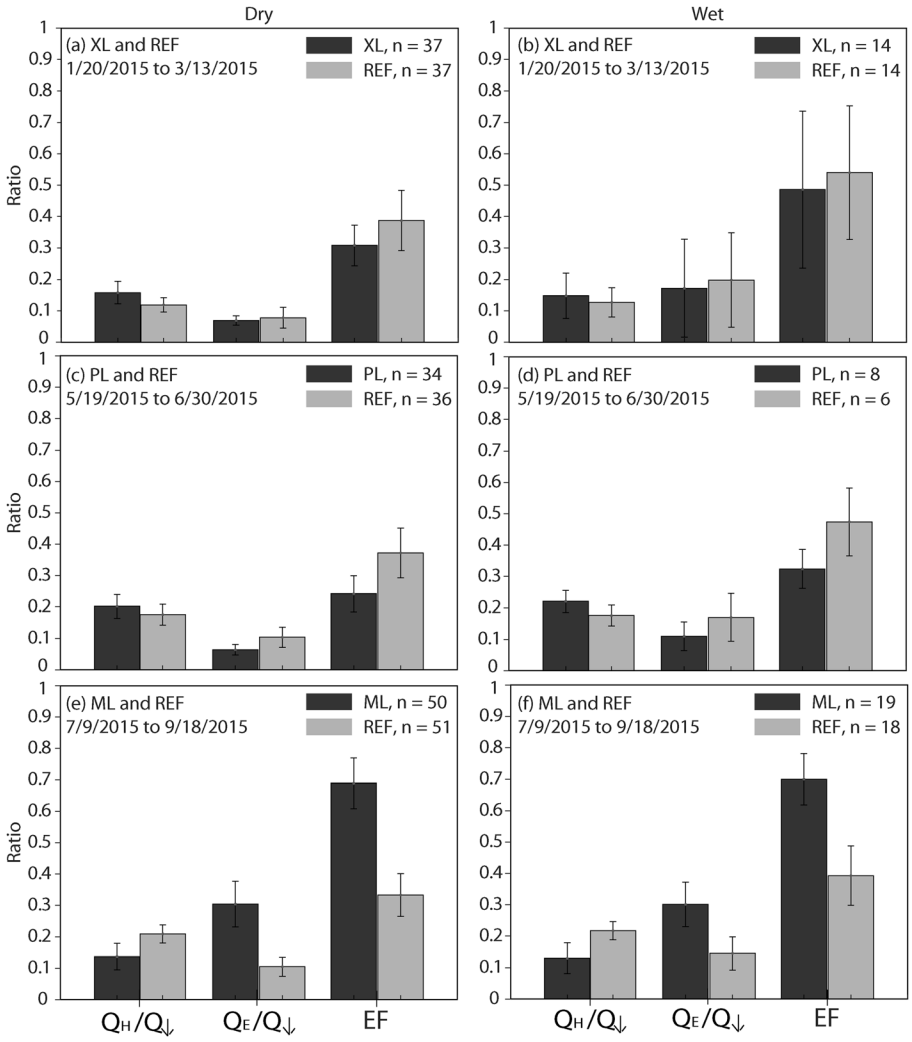

Figure 9. Comparison of averaged daily $Q_H/Q_{\downarrow}$, $Q_E/Q_{\downarrow}$ and evaporative fraction for dry (left) and wet (right) days during overlapping periods for the (a, b) xeric landscaping (XL) and suburban residential (REF) site, (c, d) parking lot (PL) and REF site, and (e, f) mesic landscaping (ML) and REF site. *n* is the number of days and the error bars represent ±1 standard deviation.

occurrence ($P > 0.2$ mm/d). Figure 9 presents the variation of $Q_H/Q_{\downarrow}$, $Q_E/Q_{\downarrow}$, and EF for wet and dry days during each season in comparison to REF. Notably, precipitation increases $Q_E/Q_{\downarrow}$ for most sites and seasons, leading to a higher EF, without a considerable change in $Q_H/Q_{\downarrow}$. This suggests that urban land covers support similar sensible heat flux under different weather conditions. The increase in latent heat flux, however, is limited to those sites and seasons with low water availability. For instance, the winter $Q_E/Q_{\downarrow}$ and EF increase at both the XL (by 0.10 and 0.18) and REF (by 0.12 and 0.15) sites due to a sequence of storm events, indicating that water-limited conditions exist despite the various types of outdoor water use at the sites. In contrast, differences are observed between the ML and REF sites with respect to their response to storm events during the NAM season. No changes in $Q_E/Q_{\downarrow}$ and EF are noted at ML (by $<$0.01 and 0.01) between dry and wet days, while increases of $Q_E/Q_{\downarrow}$ and EF occur at the REF site due to the additional water (by 0.04 and 0.06). In effect, more frequent irrigation at the ML site during the NAM season renders the partitioning of turbulent fluxes insensitive to storm events indicating that water is not limiting. It should be noted, however, that the below average rainfall at both the ML and REF sites during 2015 (Table 5) might have impacted the high degree of responsiveness of the REF sites to storm events.

We inspected the SEB and soil moisture responses to storm events to further discern the impact of outdoor water use on the sensitivity to precipitation. Figure 10 presents storms at the XL and REF sites (2–3

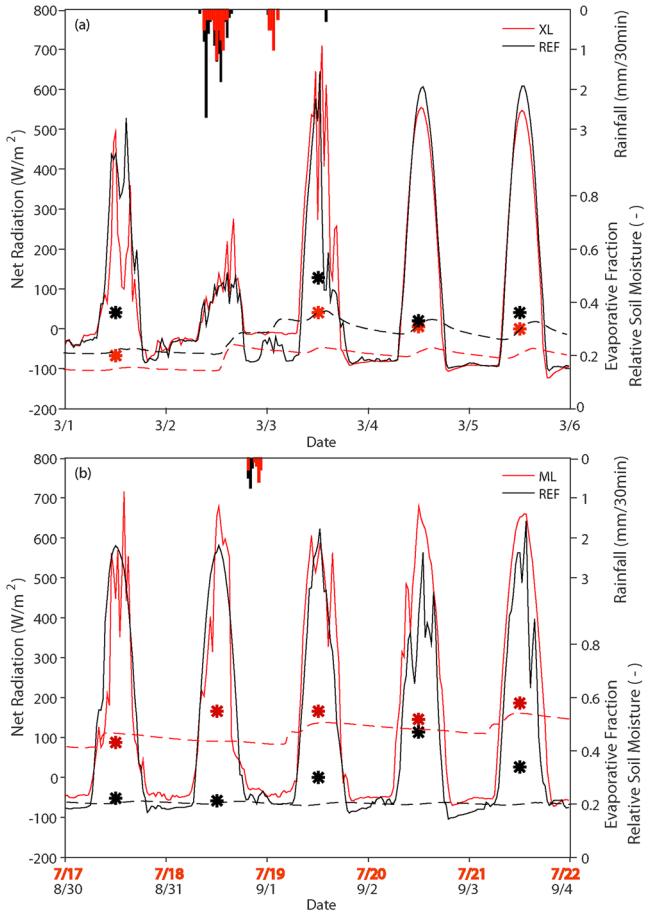

Figure 10. Comparison of precipitation (bars), net radiation (solid lines), shallow relative soil moisture (defined as volumetric soil moisture divided by porosity, with an assumed porosity value of 0.4 strictly for presentation purposes) at 5 cm depth (dashed lines) and noontime evaporative fraction (symbol) between (a) xeric landscaping (XL) and suburban residential (REF) sites during the winter deployment and (b) mesic landscaping (ML) and REF sites during the NAM season. Note that two similar events of 1.5 mm precipitation accumulation (18 July at XL and 31 August at REF) are compared in Figure 10b since simultaneous localized storms did not occur at these sites during the NAM season.

March) and the ML and REF sites (18 July and 31 August, respectively) obtained from local sensors. For each case, precipitation, net radiation, and shallow soil moisture are shown at 30 min intervals, while the daily EF is obtained as the averaged from 10:00 a.m. to 2:00 p.m (i.e., one value per day obtained near local noontime). Q^* exhibits larger variations in response to cloud cover during the winter (XL and REF sites) since the storm event occurred during daylight hours, whereas the summer storms (ML and REF sites) were both nocturnal in nature, though small variations in Q^* also occur during subsequent days. Shallow soil moisture increases a small amount in response to the storm events across the varying levels of soil water content (i.e., similar wetness at XL and REF but wetter conditions at ML than REF due to outdoor water use). More importantly, EF clearly shows a differential response among sites and seasons. For the water-limited winter conditions, the storm event led to an increase in EF at both sites of 0.13 and 0.16 (difference between EF prior to and after the storm), or 36% and 80% relative increases, lasting about 1 and 3 days at the REF and XL sites, respectively. Consistent with prior analysis, the REF site exhibited a higher EF than the XL site, though the differences are reduced during wet days. The more sensitive EF response at XL is likely due to its higher percentage (68.3%) of land cover that can absorb precipitation (e.g., grass, trees, and undeveloped land) as compared to REF (51.5%). In contrast, the summer storm events lead to an increase in EF of 0.26 at the REF site, but a small decrease of 0.01 in EF at the ML site, or relative differences of 124% and −2%, respectively. This occurs despite the higher percentage at ML (78.9%) of permeable urban land cover in the EC footprint and is closely linked to the high soil moisture conditions. Thus, the frequent outdoor water use at ML sustains a high EF that is insensitive to additional water, while the more water-limited conditions at REF allow for both responses to storm events and to outdoor water use in its larger footprint. Note that while the large increase in EF at REF on 2 September cannot be attributed to precipitation (either at the REF site or nearby rain gauges from the Flood Control District of Maricopa County), the net radiation measurements suggest the occurrence of cloud cover as confirmed by inspecting a nearby weather station from the Flood Control District of Maricopa County. Thus, the large increase in EF is likely due to a delayed reaction to nighttime precipitation on 31 August or possibly to some other outdoor water use increase at the REF site (e.g., additional irrigation input).

4. Summary and Conclusions

While model applications have indicated that the built environment impacts energy and water exchanges (e.g., Song & Wang, 2015; Wang et al., 2016), few studies have directly observed the effects of different urban land cover types on the SEB or the partitioning of turbulent fluxes. Furthermore, it is not common to test urban energy balance models against observations designed to capture the effect of variations in land cover, but see Song and Wang (2015) for an example. In this study, we conducted meteorological flux measurements using the EC technique to obtain a detailed quantification of SEB processes and relate them to the urban land cover distributions within the sampled footprints of three short-term deployments and a stationary reference site in Phoenix. Comparisons of standard weather variables, meteorological fluxes, and normalized SEB quantities between the mobile and reference sites were carried out to account for the effect of time-varying (seasonal) conditions during the short-term deployments. In addition, a comparison to long-term observations indicates that the deployments in 2015 varied to some extent as compared to the climatology at Phoenix Sky Harbor Airport, with the most important difference being the drier-than-average deployment during the NAM season. A particular focus of the analysis was placed on the comparative role of

precipitation events and outdoor water use on modifying the turbulent flux partitioning given the strong natural water limitations in the arid urban area. Results from the observational comparisons across sites, seasons, and urban land cover types indicated the following:

1. Meteorological conditions were similar between the sites but had small biases attributed to variations in vegetated land cover, with a higher TA at the REF site as compared to the XL and ML sites. Despite these similarities, large biases were noted in the time-averaged Q^*, with the REF site having values of 7 to 43 W/m^2 less than the other sites, attributed to the larger radiometer footprint and its differences in impervious surfaces and undeveloped land cover.
2. Individual radiation components and ancillary measurements provided insight into the large differences in Q^* among sites by isolating the effects of albedo on $K_{\uparrow}$ and of shallow soil temperature on L_{net}. Lower Q^* at the REF site was found to be due to either a higher albedo (relative to PL) or a higher soil temperature (relative to ML) or a combination of both factors (relative to XL).
3. The SEB revealed sharp differences in the partitioning between sensible and latent heat flux among the sites based upon normalized quantities. For instance, EF was found to be much larger in the irrigated turf grass at ML, where a higher $(Q_H + Q_E)/Q_{\downarrow}$ was also measured. Sensible heat flux, on the other hand, was the dominant flux and exhibited lower variations among the other sites, suggesting less frequent or extensive outdoor water use.
4. The sensitivity of SEB processes to precipitation events varied considerably among the sites in accordance with the soil moisture conditions established through outdoor water use. While different urban land covers support similar sensible heat flux under different weather conditions, the latent heat flux varies significantly at those locations that are water limited, whereas frequent sprinkler irrigation at ML renders the EF insensitive to additional water input.

Based upon these comparisons, key differences in the SEB among the sites can be attributed to the urban land cover contained in the measurement footprints, including the frequency and amount of outdoor water use. While the mobile deployments only sampled individual seasons, comparisons to the reference site provided an opportunity to draw the important conclusions listed above. Indeed without the reference site, it would have been difficult to distinguish between the effects of seasonality (e.g., winter at XL versus summer at ML) and of urban land cover (e.g., xeric versus mesic) on the SEB. Nevertheless, it would be desirable to conduct cross-site comparisons over a full year and to improve the correspondence in the footprint dimensions among deployments and between the scale of the radiation, turbulent, and ground heat flux measurements. In particular, heterogeneous urban environments present challenges to soil temperature observations and its effect on the SEB that could be addressed by applying techniques for inferring ground heat flux from single sensors as in Wang (2012). In addition, longer temporal comparisons could be used to evaluate if frequent or high outdoor water use effectively decouples turbulent flux partitioning from precipitation during other seasons. Furthermore, additional studies are needed to verify if the application of urban irrigation can be an effective proxy for quantifying the spatiotemporal variability of the SEB in arid urban areas. A fruitful avenue would be the validation of a numerical model that simulates urban energy and water fluxes (e.g., Grimmond & Oke, 1991; Järvi et al., 2011; Wang et al., 2013) and its subsequent application to quantify the link between urban irrigation and SEB processes. Based on this approach, considerable improvements could be made in estimating the spatiotemporal variability of the urban surface energy budget in desert cities.

Acknowledgments
Funding was provided by the U.S. Army Research Office (grant 65962-EVII) and the National Science Foundation through grant EF1049251 "Assessing Decadal Climate Change Impacts on Urban Populations in the Southwestern United States" and grant DEB-1026865 "CAPIV: Central Arizona-Phoenix Long-term Ecological Research Program." Special thanks to Ivan López-Castrillo and Thomas J. Volo for field assistance and the Facilities Department at Arizona State University (Raymond Humbert, John Herrera, and Jimmy Mastalsz) for help with securing site permits. Original data sets can be obtained at the CAP LTER Data Catalog http://sustainability.asu.edu/caplter/data/. We thank two anonymous reviewers and Darrel Jenerette for insightful comments that helped to improve an earlier version of the manuscript.

References

Adams, D. K., & Comrie, A. C. (1997). The North American monsoon. *Bulletin of the American Meteorological Society*, *78*(10), 2197–2213. https://doi.org/10.1175/1520-0477(1997)078%3C2197:TNAM%3E2.0.CO;2

Anderson, C. A., & Vivoni, E. R. (2016). Impact of land surface states within the flux footprint on daytime land-atmosphere coupling in two semiarid ecosystems of the southwestern U.S. *Water Resources Research*, *52*, 4785–4800. https://doi.org/10.1002/2015WR018016

Arnfield, A. J. (2003). Two decades of urban climate research: A review of turbulence, exchanges of energy and water, and the urban heat island. *International Journal of Climatology*, *23*(1), 1–26. https://doi.org/10.1002/joc.859

Baldocchi, D., Hicks, B. B., & Meyers, T. P. (1988). Measuring biosphere-atmosphere exchanges of biologically related gases with micrometeorological method. *Ecology*, *69*(5), 1331–1340. https://doi.org/10.2307/1941631

Bassett, R., Cai, X., Chapman, L., Heaviside, C., Thornes, J. E., Muller, C. L., et al. (2016). Observations of urban heat island advection from a high-density monitoring network. *Quarterly Journal of the Royal Meteorological Society*, *142*(699), 2434–2441. https://doi.org/10.1002/qj.2836

Benson-Lira, V., Georgescu, M., Kaplan, S., & Vivoni, E. R. (2016). Loss of a lake system in a megacity: The impact of urban expansion on seasonal meteorology in Mexico City. *Journal of Geophysical Research: Atmospheres*, *121*, 3079–3099. https://doi.org/10.1002/2015JD024102

Best, M. J., & Grimmond, C. S. B. (2016). Modelling the partitioning of turbulent fluxes at urban sites with varying vegetation cover. *Journal of Hydrometeorology*, *17*(10), 2537–2553. https://doi.org/10.1175/JHM-D-15-0126.1

Buyantuyev, A., & Wu, J. (2010). Urban heat islands and landscape heterogeneity: Linking spatiotemporal variations in surface temperatures to land-cover and socioeconomic patterns. *Landscape Ecology*, *25*(1), 17–33. https://doi.org/10.1007/s10980-009-9402-4

Buyantuyev, A., & Wu, J. (2012). Urbanization diversifies land surface phenology in arid environments: Interactions among vegetation, climate variations and land use patterns in the Phoenix metropolitan region, USA. *Landscape and Urban Planning*, *105*(1-2), 149–159. https://doi.org/10.1016/j.landurbplan.2011.12.013

Chow, W. T. L., Salamanca, F., Georgescu, M., Mahalov, A., Milne, J. F., & Ruddell, B. L. (2014). A multi-method and multi-scale approach for estimating city-wide anthropogenic heat fluxes. *Atmospheric Environment*, *99*, 64–76. https://doi.org/10.1016/j.atmosenv.2014.09.053

Chow, W. T. L., Volo, T. J., Vivoni, E. R., Jenerette, G. D., & Ruddell, B. L. (2014). Seasonal dynamics of a suburban energy balance in Phoenix, Arizona. *International Journal of Climatology*, *34*(15), 3863–3880. https://doi.org/10.1002/joc.3947

Christen, A., & Voogt, R. (2004). Energy and radiation valance of a central European city. *International Journal of Climatology*, *24*(11), 1395–1421. https://doi.org/10.1002/joc.1074

Clement, R. (1999). *EdiRe Data Software (Version 1.5.0.32)*, *Sch. Of Geosci*. Edinburgh, UK: University of Edinburgh. Retrieved from http://www.geos.ed.ac.uk/abs/research/micromet/EdiRe

Cook, E. M., Hall, S. J., & Larson, K. L. (2012). Residential landscapes as social-ecological systems: A synthesis of multi-scalar interactions between people and their home environment. *Urban Ecosystems*, *15*(1), 19–52. https://doi.org/10.1007/s11252-011-0197-0

Coutts, A. M., Beringer, J., & Tapper, N. J. (2007). Impact of increasing urban density on local climate: Spatial and temporal variations in the surface energy balance in Melbourne, Australia. *Journal of Applied Meteorology and Climatology*, *46*(4), 477–493. https://doi.org/10.1175/JAM2462.1

Foken, T. (2006). 50 years of the Monin-Obukhov similarity theory. *Boundary-Layer Meteorology*, *119*(3), 431–447. https://doi.org/10.1007/s10546-006-9048-6

Georgescu, M., Chow, W. T. L., Wang, Z. H., Brazel, A., Trapido-Lurie, B., Roth, M., & Benson-Lira, V. (2015). Prioritizing urban sustainability solutions: Coordinated approaches must incorporate scale-dependent built environment induced effects. *Environmental Research Letters*, *10*(7), 079601. https://doi.org/10.1088/1748-9326/10/7/079601

Georgescu, M. G., Miguez-Macho, L. T., & Steyaert, W. C. P. (2009). Climatic effects of 30 years of landscape change over the Greater Phoenix, Arizona, region: 1. Surface energy budget changes. *Journal of Geophysical Research*, *114*, D05110. https://doi.org/10.1029/2008JD010745

Gober, P., Brazel, A., Quay, R., Myint, S., Grossman-Clarke, S., Miller, A., & Rossi, S. (2010). Using watered landscapes to manipulate urban heat island effects: How much water will it take to cool Phoenix? *Journal of the American Planning Association*, *76*, 109–121.

Goldbach, A., & Kuttler, W. (2013). Quantification of turbulent heat fluxes for adaptation strategies within urban planning. *International Journal of Climatology*, *33*(1), 143–159. https://doi.org/10.1002/joc.3437

Grimm, N. B., Faeth, S. H., Golubiewski, N. E., Redman, C. L., Wu, J., Bai, X., & Briggs, J. M. (2008). Global change and the ecology of cities. *Science*, *319*(5864), 756–760. https://doi.org/10.1126/science.1150195

Grimmond, C. S. B. (2006). Progress in measuring and observing the urban atmosphere. *Theoretical and Applied Climatology*, *84*(1-3), 3–22. https://doi.org/10.1007/s00704-005-0140-5

Grimmond, C. S. B., & Christen, A. (2012). Flux measurements in urban ecosystems. *Fluxletter Newsletter Fluxnet*, *5*(1), 1–8.

Grimmond, C. S. B., & Oke, T. R. (1991). An evapotranspiration-interception model for urban areas. *Water Resources Research*, *27*(7), 1739–1755 . https://doi.org/10.1029/91WR00557

Grimmond, C. S. B., & Oke, T. R. (2002). Turbulent heat fluxes in urban areas: Local-scale observations and a local-scale urban meteorological parameterization scheme (LUMPS). *Journal of Applied Meteorology*, *41*(7), 792–810. https://doi.org/10.1175/1520-0450(2002)041%3C0792:THFIUA%3E2.0.CO;2

Grimmond, C. S. B., Roth, M., Oke, T. R., Au, Y. C., Best, M., Betts, R., et al. (2010). Climate and more sustainable cities: Climate information for improved planning and management of cities (producers/capabilities perspective). *Procedia Environmental Sciences*, *1*, 247–274. https://doi.org/10.1016/j.proenv.2010.09.016

Hirt, P., Gustafson, A., & Larson, K. L. (2008). The mirage in the valley of the Sun. *Environmental History*, *13*(3), 482–514. https://doi.org/10.1093/envhis/13.3.482

Hong, J.-W., & Hong, J. (2016). Changes in the Seoul metropolitan area urban heat environment with residential redevelopment. *Journal of Applied Meteorology and Climatology*, *55*(5), 1091–1106. https://doi.org/10.1175/JAMC-D-15-0321.1

Hope, D., Gries, C., Zhu, W. X., Fagan, W. F., Redman, C. L., Grimm, N. B., et al. (2003). Socioeconomics drive urban plant diversity. *Proceedings of the National Academy of Sciences of the United States of America*, *100*(15), 8788–8792. https://doi.org/10.1073/pnas.1537557100

Järvi, L., Grimmond, C. S. B., & Christen, A. (2011). The Surface Urban Energy and Water Balance Scheme (SUEWS): Evaluation in Los Angeles and Vancouver. *Journal of Hydrology*, *411*(3-4), 219–237. https://doi.org/10.1016/j.jhydrol.2011.10.001

Jenerette, G. D., Harlan, S. L., Stefanov, W. L., & Martin, C. A. (2011). Ecosystem services and urban heat riskscape moderation: Water, green spaces, and social inequality in Phoenix, USA. *Ecological Applications*, *21*(7), 2637–2651. https://doi.org/10.1890/10-1493.1

Kormann, R., & Meixner, F. X. (2001). An analytical footprint model for non-neutral stratification. *Boundary-Layer Meteorology*, *99*(2), 207–224. https://doi.org/10.1023/A:1018991015119

Kotthaus, S., & Grimmond, C. S. B. (2012). Identification of micro-scale anthropogenic CO_2 heat and moisture sources—Processing eddy covariance fluxes for a dense urban environment. *Atmospheric Environment*, *57*, 301–316. https://doi.org/10.1016/j.atmosenv.2012.04.024

Lee, T. W., Lee, J. Y., & Wang, Z. H. (2012). Scaling of the urban heat island intensity using time-dependent energy balance. *Urban Climate*, *2*, 16–24. https://doi.org/10.1016/j.uclim.2012.10.005

Liang, L. L., Anderson, R. G., Shiflett, S. A., & Jenerette, G. D. (2017). Urban outdoor water use and response to drought assessed through mobile energy balance and vegetation greenness measurements. *Environmental Research Letters*, *12*(8), 084007. https://doi.org/10.1088/1748-9326/aa7b21

Litvak, E., McCarthy, H. R., & Pataki, D. E. (2017). A method for estimating transpiration of irrigated urban trees in California. *Landscape and Urban Planning*, *158*, 48–61. https://doi.org/10.1016/j.landurbplan.2016.09.021

Litvak, E., & Pataki, D. E. (2016). Evapotranspiration of urban lawns in a semi-arid environment: An in-situ evaluation of microclimatic conditions and water recommendations. *Journal of Arid Environments*, *134*, 87–96. https://doi.org/10.1016/j.jaridenv.2016.06.016

Loridan, T., & Grimmond, C. S. B. (2012). Characterization of energy flux partitioning in urban environments: Links with surface seasonal properties. *Journal of Applied Meteorology and Climatology*, *51*(2), 219–241. https://doi.org/10.1175/JAMC-D-11-038.1

Ma, Y., Fan, S., Ishikawa, H., Tsukamoto, O., Yao, T., Koike, T., et al. (2005). Diurnal and inter-monthly variation of land surface heat fluxes over the central Tibetan Plateau area. *Theoretical and Applied Climatology*, *80*(2-4), 259–273. https://doi.org/10.1007/s00704-004-0104-1

Martin, C. A., Busse, K., & Yabiku, S. (2007). North Desert Village: The effect of landscape manipulation on microclimate and its relation to human landscape preferences. *Hortscience*, *42*, 853.

Mascaro, G. (2016). Multiscale spatial and temporal statistical properties of rainfall in central Arizona. *Journal of Hydrometeorology*, *18*, 227–245.

Massman, W. J. (2001). Reply to comment by Rannik on: "A simple method for estimating frequency response corrections for eddy covariance systems". *Agricultural and Forest Meteorology*, *107*(3), 247–251. https://doi.org/10.1016/S0168-1923(00)00237-9

Middel, A., Brazel, A. J., Gober, P., Myint, S. W., Chang, H., & Duh, J.-D. (2012). Land cover, climate, and the summer surface energy balance in Phoenix, AZ, and Portland, OR. *International Journal of Climatology*, *32*(13), 2020–2032. https://doi.org/10.1002/joc.2408

Middel, A., Chhetri, N., & Quay, R. (2015). Urban forestry and cool roofs: Assessment of heat mitigation strategies in Phoenix residential neighborhoods. *Urban Forestry & Urban Greening*, *14*(1), 178–186. https://doi.org/10.1016/j.ufug.2014.09.010

Mitchell, V. G., Cleugh, H. A., Grimmond, C. S. B., & Xu, J. (2008). Linking urban water balance and energy balance models to analyze urban design options. *Hydrological Processes*, *22*(16), 2891–2900. https://doi.org/10.1002/hyp.6868

Myint, S. W., Gober, P., Brazel, A., Grossman-Clarke, S., & Weng, Q. (2011). Per-pixel vs. object-based classification of urban land cover extraction using high spatial resolution imagery. *Remote Sensing of Environment*, *115*(5), 1145–1161. https://doi.org/10.1016/j.rse.2010.12.017

Norton, B. A., Coutts, A. M., Livesley, S. J., Harris, R. J., Hunter, A. M., & Williams, N. S. G. (2015). Planning for cooler cities: A framework to priorities green infrastructure to mitigate high temperatures in urban landscapes. *Landscape and Urban Planning*, *134*, 127–138. https://doi.org/10.1016/j.landurbplan.2014.10.018

Offerle, B., Grimmond, C. S. B., Fortuniak, K., & Pawlak, W. (2006). Intraurban differences of surface energy fluxes in a central European city. *Journal of Applied Meteorology and Climatology*, *45*(1), 125–136. https://doi.org/10.1175/JAM2319.1

Oke, T. R. (1988). The urban energy balance. *Progress in Physical Geography*, *12*, 471–508.

Paw, U. K. T., Baldocchi, D. D., Meyers, T. P., & Wilson, K. B. (2000). Correction of eddy-covariance measurements incorporating both advective effects and density fluxes. *Boundary-Layer Meteorology*, *97*(3), 487–511. https://doi.org/10.1023/A:1002786702909

Sailor, D. J. (2011). A review of methods for estimating anthropogenic heat and moisture emissions in the urban environment. *International Journal of Climatology*, *31*(2), 189–199. https://doi.org/10.1002/joc.2106

Salamanca, F., Georgescu, M., Mahalov, A., Moustaoui, M., & Wang, M. (2014). Anthropogenic heating of the urban environment due to air conditioning. *Journal of Geophysical Research: Atmospheres*, *119*, 5949–5965. https://doi.org/10.1002/2013JD021225

Santillán-Soto, N., García-Cueto, R., Haro-Rincón, Z., Ojeda-Benitez, S., Quintero-Núñez, M., & Velázquez-Limón, N. (2015). Radiation balance of urban materials and their thermal impact in Semi-Desert region: Mexicali, México study case. *Atmosfera*, *6*, 1578–1589.

Schmid, H. P. (1994). Source areas for scalars and scalar fluxes. *Boundary-Layer Meteorology*, *67*(3), 293–318. https://doi.org/10.1007/BF00713146

Schmid, H. P., Cleugh, H. A., Grimmond, C. S. B., & Oke, T. R. (1991). Spatial variability of energy fluxes in suburban terrain. *Boundary-Layer Meteorology*, *54*(3), 249–276. https://doi.org/10.1007/BF00183956

Shaffer, S. R., Chow, W. T. L., Georgescu, M., Hyde, P., Jenerette, G. D., Mahalov, A., et al. (2015). Multiscale modeling and evaluation of urban surface energy balance in the Phoenix metropolitan area. *Journal of Applied Meteorology and Climatology*, *54*(2), 322–338. https://doi.org/10.1175/JAMC-D-14-0051.1

Song, J., & Wang, Z. H. (2015). Impacts of mesic and xeric urban vegetation on outdoor thermal comfort and microclimate in Phoenix, AZ. *Building and Environment*, *94*, 558–568. https://doi.org/10.1016/j.buildenv.2015.10.016

Stewart, I. D., & Oke, T. R. (2012). Local climate zones for urban temperature studies. *Bulletin of the American Meteorological Society*, *93*(12), 1879–1900. https://doi.org/10.1175/BAMS-D-11-00019.1

Stull, R. B. (1988). *An introduction to boundary layer meteorology* (p. 670). Dordrecht, Netherlands: Kluwer Academic. https://doi.org/10.1007/978-94-009-3027-8

Templeton, R. C., Vivoni, E. R., Mendez-Barroso, L. A., Pierini, N. A., Anderson, C. A., Rango, A., et al. (2014). High-resolution characterization of a semiarid watershed: Implications on evapotranspiration estimates. *Journal of Hydrology*, *509*, 306–319. https://doi.org/10.1016/j.jhydrol.2013.11.047

United Nations (2015). Department of economic and social affairs, population division. In *World urbanization prospects: The 2014 Revision*, *ST/ESA/SER.A/366* (p. 493). United Nations, New York.

U.S. Census Bureau (2010). 2010 Census Data. Retrieved from http://2010.census.gov/2010censusdata/data/

Van de Boer, A., Moene, A. F., Schuttemeyer, D., & Graf, A. (2013). Sensitivity and uncertainty of analytical footprint models according to a combined natural tracer and ensemble approach. *Agricultural and Forest Meteorology*, *169*, 1–11. https://doi.org/10.1016/j.agrformet.2012.09.016

Vivoni, E. R., Moreno, H. A., Mascaro, G., Rodriguez, J. C., Watts, C. J., Garatuza-Payan, J., & Scott, R. L. (2008). Observed relation between evapotranspiration and soil moisture in the North American monsoon region. *Geophysical Research Letters*, *35*, L22403. https://doi.org/10.1029/2008GL036001

Volo, T. J., Vivoni, E. R., Martin, C. A., Earl, S., & Ruddell, B. L. (2014). Modelling soil moisture, water partitioning and plant water stress under irrigated conditions in desert urban areas. *Ecohydrology*, *7*, 1297–1313.

Volo, T. J., Vivoni, E. R., & Ruddell, B. L. (2015). An ecohydrological approach to conserving urban water through optimized landscape irrigation schedules. *Landscape and Urban Planning*, *133*, 127–132. https://doi.org/10.1016/j.landurbplan.2014.09.012

Wang, Z. H. (2012). Reconstruction of soil thermal field from a single depth measurement. *Journal of Hydrology*, *464-465*, 541–549. https://doi.org/10.1016/j.jhydrol.2012.07.047

Wang, Z. H., Bou-Zeid, E., & Smith, J. A. (2013). A coupled energy transport and hydrological model for urban canopies evaluated using a wireless sensor network. *Quarterly Journal of the Royal Meteorological Society*, *139*(675), 1643–1657. https://doi.org/10.1002/qj.2032

Wang, J., & Mitsuta, Y. (1992). Evaporation from the desert: Some preliminary results of HEIFE. *Boundary-Layer Meteorology*, *59*(4), 413–418. https://doi.org/10.1007/BF02215461

Wang, Z. H., Zhao, X., Yang, J., & Song, J. (2016). Cooling and energy saving potentials of shade trees and urban lawns in a desert city. *Applied Energy*, *161*, 437–444. https://doi.org/10.1016/j.apenergy.2015.10.047

Webb, E. K., Pearman, G. I., & Leuning, R. (1980). Correction of flux measurements for density effects due to heat and water vapor transfer. *Quarterly Journal of the Royal Meteorological Society*, *106*(447), 85–100. https://doi.org/10.1002/qj.49710644707

Wilczak, J. M., Oncley, S. P., & Stage, S. A. (2001). Sonic anemometer tilt correction algorithms. *Boundary-Layer Meteorology*, *99*(1), 127–150. https://doi.org/10.1023/A:1018966204465

Wilson, K., Goldstein, A., Falge, E., Aubinet, M., Baldocchi, D., Berbigier, P., et al. (2002). Energy balance closure at FLUXNET sites. *Agricultural and Forest Meteorology*, *113*(1-4), 223–243. https://doi.org/10.1016/S0168-1923(02)00109-0

Wu, J., Jenerette, G. D., Buyantuyev, A., & Redman, C. L. (2011). Quantifying spatiotemporal patterns of urbanization: The case of the two fastest growing metropolitan areas in the United States. *Ecological Complexity*, *8*(1), 1–8. https://doi.org/10.1016/j.ecocom.2010.03.002

Yang, J., & Wang, Z. H. (2015). Optimizing urban irrigation schemes for the trade-off between energy and water consumption. *Energy and Buildings*, *107*, 335–344. https://doi.org/10.1016/j.enbuild.2015.08.045

Yang, J., Wang, Z. H., Georgescu, M., Chen, F., & Tewari, M. (2016). Assessing the impact of enhanced hydrological processes on urban hydrometeorology with application to two cities in contrasting climates. *Journal of Hydrometeorology*, *17*(4), 1031–1047. https://doi.org/10.1175/JHM-D-15-0112.1

Zhao, Q., Myint, S. W., Wentz, E. A., & Fan, C. (2015). Rooftop surface temperature analysis in an urban residential environment. *Remote Sensing*, *7*(12), 12,135–12,159. https://doi.org/10.3390/rs70912135